Available online at www.sciencedirect.com
ScienceDirect
International Journal of Hydrogen Energy 32 (2007) 3887–3898
International Journal of HYDROGEN ENERGY
www.elsevier.com/locate/ijhydene

Analysis of parameter effects on transport phenomena in conjunction with chemical reactions in ducts relevant for methane reformers

Jinliang Yuan[a,*], XinRong Lv[b], Bengt Sundén[a], Dantin Yue[b]

[a]*Department of Energy Sciences, Faculty of Engineering, Lund University, Box 118, 22100 Lund, Sweden*
[b]*Marine Engineering College, Dalian Maritime University, Dalian 116026, China*

Received 15 November 2006; received in revised form 8 March 2007; accepted 23 May 2007
Available online 16 July 2007

Abstract

Various transport phenomena in conjunction with chemical reactions are strongly affected by reformer configurations and properties of involved porous catalyst layers. The considered composite duct is relevant for a methane steam reformer and consists of a porous layer for the catalytic chemical reactions, the fuel gas flow duct and solid plate. In this paper, a fully three-dimensional calculation method is developed to simulate and analyze reforming reactions of methane, with purpose to reveal the importance of design and operating parameters grouped as three characteristic ratios. The reformer conditions such as mass balances associated with the reforming reactions and gas permeation to/from the porous catalyst reforming layer are applied in the analysis. The results show that the characteristic ratios have significant effects on the transport phenomena and overall reforming reaction performance.

Keywords: Transport phenomena; Chemical reaction; Analysis; Parameter effect; Reformer

1. Introduction

External fuel reformers/processors should be employed into the proton exchange membrane fuel cell (PEMFC) systems, because PEMFCs essentially need pure hydrogen as a fuel. Availability of highly compact hydrogen generators will make possible electrical power generation by PEMFCs at central stations, substations, or residences [1,2]. There are increasing interests worldwide in the development of innovative fuel processing technologies for fuel cell systems, for instance, compact reformers (CR hereafter) for a variety of applications. The basic idea of the CR is, by applying thin coatings of catalyst, to catalytically activate both sides of a compact heat exchanger—one side for combustion to provide heat for the other side to sustain steam reforming of methane and produce hydrogen. In this configuration, the thin coating results in small thermal conduction and species transport path lengths, and an improved utilization of the intrinsic reforming catalyst kinetics is allowed to achieve an efficient transfer of thermal energy. The compact reformer concept and its potential high power density could lead to major applications in fuel cell systems for stationary and transportation applications [3,4]. An excellent review can be found in [5] regarding the CR concept application and new design development.

Understanding of various gas and heat transport processes is crucial for increasing methane conversion, reducing manufacturing cost, and accelerating commercialization of CR. It is clear that, in the porous layer, the transport rate of fuel gases is controlled by various parameters, such as its microstructure (e.g., pore size, permeability, volume percent porosity), pressure gradient between the gas flow duct and porous layer, gas composition, and inlet conditions, etc. Several aspects (functional catalyst, support material, reactor configuration/design, and operating conditions) have been investigated theoretically in [5,6], but mainly for overall reformer performance based on simplified one- or two-dimensional approaches. Literature review shows that the researches on the analysis of parameter effects on transport phenomena are very limited [7].

In this study, various fundamental phenomena and parameter effects are investigated, with the purpose to provide

* Corresponding author. Tel.: +46 46 2224813; fax: +46 46 2224717.
E-mail address: Jinliang.yuan@vok.lth.se (J. Yuan).

0360-3199/$ - see front matter © 2007 International Association for Hydrogen Energy. Published by Elsevier Ltd. All rights reserved.
doi:10.1016/j.ijhydene.2007.05.037

Nomenclature

a	width of fuel flow duct, m
b	width of porous catalyst layer, m
c_p	specific heat, J/(kg K)
D	diffusion coefficient of species, m^2/s
D_h	hydraulic diameter, m
D_{hr}	hydraulic diameter ratio
h	overall height of the duct, m; enthalpy, kJ/mol
h_d	height of the fuel flow duct, m
h_p	thickness of porous catalyst layer, m
h_r	thickness ratio (h_p/h)
J	reaction related molar flux, $mol/(m^2\,s)$
k	thermal conductivity, W/(mK); kinetic rate constant, $kmol/(kg_{cat}h)$
K_e	equilibrium constants, Pa^2
L	reformer length, m
m_{cl}	catalyst loading, kg_{cat}/m^3
$\dot{m}$	mass diffusion flux, $kg/(m^2\,s)$
$\dot{n}$	molar diffusion flux, $mol/(m^2\,s)$
M	molecular weight of species, kg/mol
P	pressure, Pa
PL_r	permeation length ratio
PR_r	permeation rate ratio
q	heat flux, $W/(m^2)$
R	reaction rate, $kmol/(m^3\,s)$
$\Re$	gas constant, kJ/(mol K)
r_e	effective radius, m
Re	Reynolds number (UD_h/ν)
S	source term
T	temperature, °C
$\mathbf{V}$	velocity vector, m/s
V_i	velocity components in x, y and z directions, respectively, m/s
x, y, z	Cartesian coordinates
X	molar fraction of fuel species
Y	mass fraction of fuel species

Greek symbols

β	permeability of porous layer, m^2
ε	porosity
μ	dynamic viscosity, kg/(m s)
ν	kinematic viscosity, m^2/s
ρ	density, kg/m^3
τ	tortuosity

Superscripts

+	forward reaction
−	reverse reaction

Subscripts

di	diffusion
eff	effective parameter
f	fuel gas mixture
form	formation
gm	fuel gas mixture
CH_4	methane
CO	carbon monoxide
CO_2	carbon dioxide
H_2	hydrogen
H_2O	water
in	inlet
k	Knudsen diffusion
m	mass transfer
p	permeation
r	steam reforming reaction
re	reverse methanation reaction
s	solid wall; shift reaction

improved understanding and to supply guidance for the practical implementation of such a design [8]. The reformer conditions such as the combined thermal boundary conditions (heat flux on the active solid wall and thermal insulation on the other solid walls), mass balances associated with the reforming reactions, and gas permeation to/from the porous catalyst layer are applied in the analysis. Momentum and heat transport together with fuel gas species equations have been solved with coupled source terms and variable thermo-physical properties (such as density, viscosity, specific heat, etc.) of the fuel gas mixture. Based on three characteristic ratios proposed in this paper, studies have been conducted for various engineering parameters which are relevant for the CR design, and effects on the transport processes in conjunction with chemical reactions are presented and discussed in terms of various parameters, such as the species distributions, chemical reaction rates, and overall methane conversion, etc.

2. Problem statement

There are several transport processes (such as mass, heat, and momentum transport) together with chemical reactions appearing in multifunctional reactor duct. It is often found that the endothermic and exothermic reactions, such as hydrocarbon cracking, steam reforming and dehydrogenation, are strongly coupled by heat transfer in the reactors.

A three-dimensional computational fluid dynamics (CFD) code was used to simulate a methane reforming duct from a typical CR, as shown in Fig. 1. The V_i is the velocity component in the x, y, or z directions. In this study, the porous catalyst layer is assumed to be homogeneous and characterized by effective parameters and the fuel in the porous layer is in thermal equilibrium with the solid matrix. The reforming reactions take place within the catalyst porous layer. A constant flow rate $U = U_{in}$ with fixed mole fractions of the mixed fuel is specified

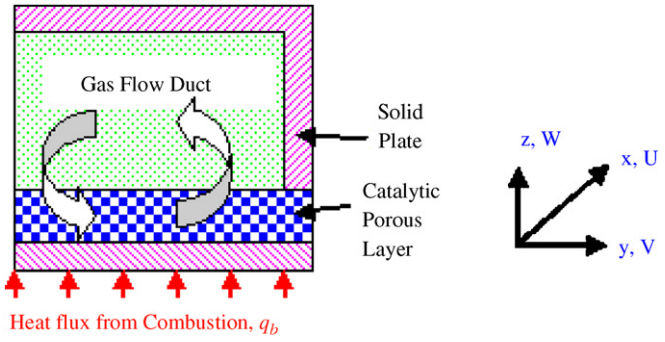

Fig. 1. Scheme of an investigated duct appeared in steam reforming reactors.

at the inlet of the fuel flow duct, while $U = 0$ is specified at the inlet for the solid walls and the porous catalyst layer. Only half of the duct is considered by imposing symmetry conditions on the mid-plane, as shown in Fig. 1.

Fundamental studies of forced convective heat transfer and gas flow, where the porous media appear, have been considered by various investigators in recent years, see [5–10]. Because of the simplicity and reasonable performance within a certain range of applications, the Darcy model has been used for the majority of existing studies on gas flow and heat transfer in porous media. For a single-phase fully developed flow through a porous medium, the Darcy model has a linear feature, i.e., the volumetrically averaged velocity in any direction in space is proportional to the pressure gradient in that direction, and inversely proportional to the viscosity. It was revealed in [8] that heat transfer can be significantly affected by the effective thermal conductivity and Darcy number of the porous medium. Various types of interfacial conditions between a porous medium and a gas flow duct were analyzed in detailed for both gas flow and heat transfer in [9]. It is clear that part of the gas flow penetrates into the porous layer and the remaining gas flows downstream at decreasing flow rates. The static pressure in such a duct then changes along the main flow due to the following reasons: the friction between the gas flow and the internal surfaces of the duct creates pressure drop, and the mass permeation (penetration of fuel gas species by convection and diffusion) across the interface between the flow duct and the porous layer implies that mass and momentum are transferred from/into the porous layer [10]. The latter one complicates the transport processes further even in a simple duct flow, because it is a mass changing process and depends on the pressure gradient between the flow duct and porous layer.

3. Various transport processes and mathematical modeling

3.1. Governing equations and source terms

In a catalytic reformer, there are many reactions and transport processes taking place. The governing equations to be solved are the mass, momentum, energy and species conservation equations. The mass continuity equation is written as

$$\nabla \bullet (\rho_{\text{eff}} \mathbf{V}) = 0. \tag{1}$$

The momentum equation reads

$$\nabla \bullet (\rho_{\text{eff}} \mathbf{V}\mathbf{V}) = -\nabla P + \nabla \bullet (\mu_{\text{eff}} \nabla \mathbf{V}) + S_{\text{di}}. \tag{2}$$

The inclusion of the source term S_{di} allows Eq. (2) to be valid for both the porous catalytic layer and the fuel gas flow duct:

$$S_{\text{di}} = -(\mu_{\text{eff}} \mathbf{V}/\beta). \tag{3}$$

This accounts for the linear relationship between the pressure gradient and flow rate according to Darcy's law. β is the porous layer permeability, and $\mathbf{V}$ represents the volume-averaged velocity vector of the species mixture. For example, the volume-averaged velocity component U in the x direction is equal to εU_{p}, where ε is the porosity and U_{p} is the average pore velocity (or interstitial velocity).

In the fuel (or gas) flow duct, the source term S_{di} becomes zero because the permeability β is infinite. Eq. (2) then reduces to the regular Navier–Stokes equation. For the porous layer, the source term is not zero. For more details, see [9] and the references included there.

Based on the thermal equilibrium assumption for the porous catalyst layer, only one energy equation is solved for the fuel gas species and the solid matrix:

$$\rho_{\text{eff}} c_{\text{p,eff}} \nabla \bullet (\mathbf{V}T) = \nabla \bullet \left(k_{\text{eff}} \nabla T - \sum_{i=1}^{n} \dot{\mathbf{m}}_i h_i \right) + S_T. \tag{4}$$

Eq. (4) balances the convected energy, the heat conduction through the solid and the fuel gas mixture, the energy due to fuel gas species diffusion, and a source term S_T. In Eq. (4) h_i is the partial enthalpy of the ith species and is obtained from [11]:

$$h_i = h_{\text{form},i} + \int_{T_0}^{T} c_{\text{pi}}(T)\,\mathrm{d}T, \tag{5}$$

where $h_{\text{form},i}$ is the specific enthalpy of formation of the ith gas species at $T = T_0 = 298.15\,\text{K}$. The heat source term S_T in Eq. (4) is associated with the steam reforming, water gas-shift and reverse methanation reactions (more discussion in the forthcoming sections),

$$S_T = \sum_i R_i \Delta h_{\text{reaction},i}, \tag{6}$$

where R_i is the reaction rate, and $\Delta h_{\text{reaction},i}$ is the reaction enthalpy.

The species mass conservation equations are written in the general form,

$$\nabla \bullet (\rho_{\text{eff}} \mathbf{V} Y_i) = \nabla \dot{m}_i + S_{s,i}, \tag{7}$$

where Y_i is the mass fraction of the ith fuel gas species, $\dot{m}_i$ represents the mass diffusive flux of species, and $S_{s,i}$ the production/consumption rate of the ith fuel species. The above equation is solved for H_2, CH_4, CO, and H_2O, respectively, i.e., for $n - 1$ species where n is the total number of species involved in the fuel gas mixture. The mass fraction of the nth species

(CO_2) can be obtained from the requirement that the sum of the mass fractions equals one.

Mass diffusion is a process leading to equalization of substance fraction or establishing an equilibrium gas distribution that results from random migration of the species. Molecular diffusion occurs as a result of thermal motion of the molecules, and the flux of the species i is proportional to the fraction gradient and diffusion coefficient. One of the significant challenges in fuel reforming modeling is in determining the rate at which the species diffuse and gases convect in the fuel flow ducts and porous catalytic areas. This requires knowledge of multi-component diffusion in the fuel flow ducts, particularly in the porous catalytic layers. In the literature, there are several basic approaches for determining the molar diffusion flux $\dot{n}_i$ and converting to mass diffusion flux $\dot{m}_i$ via the species molar mass, i.e., $\dot{n}_i = \dot{m}_i/M_i$ [7]. A multi-component mixture extension of Fick's law is sometimes used in the literature as well, e.g., in [13], and also applied in this study,

$$\dot{n}_i = -\rho D_{i,\mathrm{gm}} \nabla X_i + X_i \sum_{i=1}^{n} \dot{n}_j. \tag{8}$$

The diffusion coefficients of species i in the gas mixture for the fuel gas flow duct are calculated by the expression based on the binary coefficients [11]

$$D_{A,\mathrm{gm}} = \frac{1 - X_A}{X_B/D_{AB} + X_C/D_{AC} + \cdots}, \tag{9}$$

where $D_{A,\mathrm{gm}}$ is the diffusion coefficient of the component A in the mixture with $B, C, \ldots, X_A, X_B, X_C$ are the molar fraction of the appropriate species, and D_{AB} and D_{AC} are the diffusion coefficients in the AB and AC binary system, respectively. It is clear that for an n component system, $n(n-1)/2$ binary diffusivities are required.

For the porous catalytic reaction region, molecular diffusion is predominant in the case with large pores, whose size is much bigger than the mean free-path of the diffusion gas molecules. In this case, diffusion can be described as presented above for the fuel flow duct. Knudsen diffusion occurs in porous layer with small pores or under low pressure when the mean free-path of molecules is larger than the pore size, and the molecules collide with the walls more often than between themselves. In order to calculate the Knudsen diffusion flux, the coefficient $D_{i,\mathrm{k}}$ is calculated based on the free molecule flow theory [12]:

$$D_{i,\mathrm{k}} = \frac{2}{3} r_{\mathrm{e}} v_i = \frac{2}{3} r_{\mathrm{e}} \left(\frac{8\Re T}{\pi M_i} \right), \tag{10}$$

in which r_{e} is the effective radius and v_i the average molecular speed of the ith gas species. To account for the reduction in the cross-sectional area and the increased diffusion length due to the tortuous paths of real pores in the porous catalytic layer, the effective diffusion coefficient can be evaluated [5,11]:

$$D_{i,\mathrm{eff}} = \frac{\varepsilon}{\tau} \left(\frac{D_{i,\mathrm{gm}} \times D_{i,\mathrm{k}}}{D_{i,\mathrm{gm}} + D_{i,\mathrm{k}}} \right), \tag{11}$$

where ε is the porous porosity, and τ the tortuosity.

In Eq. (7), the source terms $S_{s,i}$ read:

$$S_{\mathrm{s,H_2}} = (3R_1 + R_2 + 4R_3) M_{\mathrm{H_2}};$$

$$S_{\mathrm{s,CH_4}} = (-R_1 - R_3) M_{\mathrm{CH_4}};$$

$$S_{\mathrm{s,H_2O}} = (-R_1 - R_2 - 2R_3) M_{\mathrm{H_2O}};$$

$$S_{\mathrm{s,CO}} = (R_{\mathrm{r}} - R_{\mathrm{s}}) M_{\mathrm{CO}}, \tag{12}$$

where R_i is the chemical reaction rate expressed by following Eqs. (16)–(18).

3.2. Boundary and interfacial conditions

Based on the reforming reaction function, the thermal and fuel gas mass fraction/flux boundary conditions at the walls are employed in this study, see [7] for details. It should be noted that the heat input to the steam reforming duct is from the catalytic combustion zone, which is not included yet in this study, and the supplied heat is then considered as a constant value of the heat flux q_{b} at the bottom wall, see Fig. 1.

3.3. Characteristic ratios

Three characteristic ratios, having significant effects on various transport processes and chemical reactions as discussed later in this paper, are defined in this section. These are the hydraulic diameter ratio D_{hr} (ratio of the porous layer diameter to the flow duct diameter), the permeation length ratio $\mathrm{PL_r}$ (ratio of the fuel flow duct width to the porous catalyst layer width), and the permeation rate ratio $\mathrm{PR_r}$ (ratio of the entrance pressure gradient to permeation resistance).

$$D_{\mathrm{hr}} = D_{\mathrm{hp}}/D_{\mathrm{hd}}, \tag{13}$$

$$\mathrm{PL_r} = a/b, \tag{14}$$

$$\mathrm{PR_r} = (\rho U_{\mathrm{in}}^2/2h_{\mathrm{p}})/(\mu U_{\mathrm{in}}/\beta_i) = (\rho \beta_i U_{\mathrm{in}})/(2\mu h_{\mathrm{p}}). \tag{15}$$

D_{hp} in Eq. (13) is the hydraulic diameter of the porous catalyst layer, D_{hd} the hydraulic diameter of the fuel flow duct; a in Eq. (14) is the width of gas flow duct, b the width of the porous catalyst layer; h_{p} in Eq. (15) is the thickness of the porous layer. It is clear that both diameter ratio D_{hr} and permeation length ratio $\mathrm{PL_r}$ are related to the fuel flow duct and catalytic porous layer configurations, to account for the characteristics of the permeation area and length, respectively. The permeation rate ratio $\mathrm{PR_r}$ considers the characteristics of the catalytic porous material (such as the permeability β_i) and duct operation parameter (such as the inlet velocity U_{in}).

4. Chemical reactions and modeling

As revealed in [1,5,6], the steam reforming, water gas-shift, and reverse methanation reactions of methane are the major ones with significant reaction rates, while other side reactions include cracking of methane and carbon monoxide resulting in carbon deposition, and gasifying carbon by steam with very low reaction rates. Consequently, the above mentioned side

reactions can be ignored, and only the following major chemical reactions are included in this study:

Methane steam reforming: $CH_4 + H_2O \rightarrow CO + 3H_2$,

$$\Delta h_{(298\,K)} = 226\,000\,\text{kJ/kmol}, \tag{16}$$

Water gas-shift: $CO + H_2O \rightarrow CO_2 + H_2$,

$$\Delta h_{(298\,K)} = -41\,000\,\text{kJ/kmol}, \tag{17}$$

Reverse methanation: $CH_4 + 2H_2O \rightarrow CO_2 + 4H_2$,

$$\Delta h_{(298\,K)} = 16\,5000\,\text{kJ/kmol}. \tag{18}$$

It should be mentioned that the above processes in Eqs. (16) and (18) are endothermic and the overall balance of the reactions requires net heat input. In general, this heat supply depends on the thermal integration methods employed and the associated combustion processes, its value is implemented by a constant heat flux q_b in this study, as shown in Fig. 1.

A general rate equation based on Langmuir–Hinselwood–Hougen–Watson (LHHW) approach [5,14] describes most accurately the process for a wide range of parameters, and is applied in this study to express the kinetic rates of absorption or production of the gas species, based on partial pressure, temperature and species compositions for the chemical reactions (16)–(18):

$$R_1 = \frac{k_1/p_{H_2}^{2.5}(p_{CH_4}p_{H_2O} - p_{H_2}^3 p_{CO}/K_{e,1})}{(\text{Den})^2} m_{cl},$$

$$\text{kmol}/(\text{m}^3\,\text{s}), \tag{19}$$

$$R_2 = \frac{k_2/p_{H_2}(p_{CO}p_{H_2O} - p_{H_2}p_{CO_2}/K_{e,2})}{(\text{Den})^2} m_{cl},$$

$$\text{kmol}/(\text{m}^3\,\text{s}), \tag{20}$$

$$R_3 = \frac{k_3/p_{H_2}^{3.5}(p_{CH_4}p_{H_2O}^2 - p_{H_2}^4 p_{CO_2}/K_{e,3})}{(\text{Den})^2} m_{cl},$$

$$\text{kmol}/(\text{m}^3\,\text{s}), \tag{21}$$

in which, m_{cl} is the catalyst loading ($\text{kg}_{cat}/\text{m}^3$), and $\text{Den} = 1 + K_{CO}p_{CO} + K_{H_2}p_{H_2} + K_{CH_4}p_{CH_4} + K_{H_2O}p_{H_2O}/p_{H_2}$. The values of the pre-exponential factors, activation energies, equilibrium constants, and heat of adsorption are given in [7]. The most common industrial catalyst is based on Ni on alumina support, with Ni content 7–15% [5]. An important aspect of catalyst design and performance analysis concerns net catalyst loading or/and effective surface area. It is preferable to use a parameter like the specific surface area, i.e., the active surface area per unit volume of porous catalyst structure. The reaction rates can be stated per unit area of catalyst surface, which is independent of the particular support structure and catalyst loading. Due to the lack of available data for the specific surface area, however, the net catalyst loading is specified as a relevant parameter for the analysis in this study.

5. Numerical solution methodology

As discussed above, the equations needed for the calculation are coupled by temperature, partial pressure/fraction of gas species via source terms and thermal–physical properties. It is clear that no gas flow is present in the solid plates. Eqs. (1), (2), and (7) are then blocked out and only the heat conduction equation, derived from the energy Eq. (4), is solved for this domain. As mentioned earlier, the thermal–physical properties of the gas mixture are variable. These parameters depend on the position in the duct, and the species mass fraction and/or temperature as well. Fuel gas mixture density, viscosity, and specific heat are then calculated and updated during the calculations.

A three-dimensional CFD code was applied to solve the governing Eqs. (1), (2), (4), and (7), together with the boundary conditions and interfacial conditions (see [7]). The code was developed for a general purpose, and is based on the finite-volume technique with boundary fitted coordinates for solving the differential equations. The momentum equations are solved for the velocity components on a non-staggered grid arrangement. The Rhie–Chow [15] interpolation method is used to compute the velocity components at the control volume faces. Algorithms based on the TDMA (tri-diagonal matrix algorithm) and a modified SIP (strongly implicit procedure) are employed for solving the algebraic equations. In this study, the convective terms are treated by the QUICK (quadratic upstream interpolation convective kinematics) scheme, while the diffusive terms are treated by the central difference scheme. The SIMPLEC (SIMPLE-Consistent) algorithm handles the linkage between velocities and pressure. A uniform grid point distribution over the cross section is used. To obtain finer meshes in the entrance region of the duct, a non-uniform distribution of grid points with an expansion factor is implemented for the main flow direction. In order to evaluate the performance of the numerical method and code, test calculations considering grid sensitivity, code performance and validation were carried out. It has been found that the predictions do not change significantly in terms of fuel species distributions, when the number of grid points is increased beyond $70 \times 70 \times 50$ (70×50 for the cross section, 70 for the main flow direction). Calculations have been carried out for fully developed conditions in a parallel plate duct for various thicknesses of the porous layer and the same boundary conditions of constant heat flux on the walls. The comparison shows that the computed values of Nusselt numbers *Nu* agree well with the analytical ones in [16].

6. Results and discussion

Configuration and operating parameters of a typical reforming duct are applied as a base case in this study [7]. Table 1 shows the base geometry parameters. For the porous layer, the parameters are chosen as: porosity $\varepsilon = 0.5$, permeability $\beta = 2 \times 10^{-10}\,\text{m}^2$, and catalyst loading $m_{cl} = 1\,\text{g}_{cat}/\text{cm}^3$. Based on the base case data above, the three characteristics ratios are $D_{hr} = 1.07$, $\text{PL}_r = 0.8$ and $\text{PR}_r = 0.042$, respectively. It should be noted that the results presented hereafter are for

various ratios by changing h_d, a, h_p, b and U_{in}, respectively. The binary diffusion coefficients of the fuel species are shown in [7]. Fuel inlet temperature $T_{in} = 650\,^{\circ}C$; inlet mole fraction $H_2: CH_4: CO: H_2O: CO_2 = 0.026: 0.2470: 0: 0.7145: 0.0125$ with $U_{in} = 5\,m/s$.

In this section, the main results of the numerical simulations are reported and discussed. The transport processes and reforming performance are presented in terms of velocity profiles, species mass fraction, chemical reaction rate and temperature profiles for the characteristic ratios, i.e., the diameter ratio D_{hr}, the permeation length ratio PL_r, and the permeation rate ratio PR_r.

6.1. Effects of the diameter ratio ($D_{hr} = 1.17, 0.99$ vs. 1.07)

To investigate effects of the diameter ratio on the transport phenomena and reformer performance, the height of fuel flow duct h_d was varied. Fig. 2 shows velocity contours for the cases of $D_{hr} = 1.17$ ($h_d = 3.5$ mm) and $D_{hr} = 0.99$ ($h_d = 4.5$ mm). As shown by dashed lines, the base case ($D_{hr} = 1.07$, $h_d = 4$ mm) is present as well in Fig. 2. It should be noted that the height of the upper solid plate was changed accordingly to keep the total height of the upper solid plate and the fuel flow duct constant.

As claimed in [7] for the base case condition, the uniform distribution and the symmetry of the axial velocity associated with a pure forced duct flow do not exist any more, and the position of the maximum values shifts away from the central plane. On the other hand, the velocity in the catalyst porous layer is very small except in the region close to the fuel flow duct, because the gas penetration into the porous layer is weak.

Table 1
Geometries of the reforming reaction duct (cm)

	Length $L(x)$	Depth $h(y)$	Width a or $b(z)$
Overall duct	20	1	0.5
Fuel flow duct	20	0.4	0.4
Porous catalytic layer	20	0.4	0.5

A small convective gas flow is identified only in the porous catalytic layer close to the fuel flow duct. As shown in Fig. 2, the velocity contours for big or small D_{hr} have a similar trend as that of the base case, i.e., there is no symmetry of the axial velocity and the position of the maximum values (1.45 vs. 1.54 m/s in Figs. 2a and b, respectively) shifts away from the physically central plane. This effect is more significant for the big D_{hr} case (shown in Fig. 2a), if compared to the one with small D_{hr} (shown in Fig. 2b). More critically, more fuel is permeated to and kept in the porous reaction region, as shown in Fig. 2a with smaller velocity contours (1.45 m/s) than those in Fig. 2b (1.54 m/s). This may be due to the fact that the fuel flow duct in Fig. 2a is small if compared to the porous catalyst layer.

As discussed in [7] for the base case condition, the steam reforming reaction is strong in the interface region of the porous catalyst layer close to the fuel flow duct (with big reaction rate value), and weak in the rest of the porous layers. For the water gas-shift reaction in Eq. (17), the reaction rate is small compared to the other two reactions in all the reaction regions. On the other hand, the reverse methanation reaction is strong in the interface region of the porous catalyst layer close to the fuel flow duct, and weak in the rest of the porous layers, as shown in [7]. However, almost the same steam reforming reaction rates are obtained in Fig. 3, when the diameter ratio changes. This finding is also true for the water gas-shift reaction and the reverse methanation reaction, in terms of maximum reaction rates (around 0.0001 and 1.20 kmol/(m^3 s), respectively) as shown in Table 2. This means that the diameter ratio has more significant effects on the fuel gas flow in both fuel flow duct and the porous catalyst layer than those on the chemical reactions. It is believed that the high methane conversion (94.48%) obtained in the case of big D_{hr} is mainly due to the fact that the fuel flow rate is small when the fuel flow duct is small or the diameter ratio D_{hr} is big.

It should be noted that the methane conversion efficiency is defined in the conventional manner, i.e., the ratio of mole CH_4 fraction difference between the reformer inlet and exit, and the fraction at the inlet, $(X_{CH_4,inlet} - X_{CH_4,exit})/X_{CH_4,inlet}$.

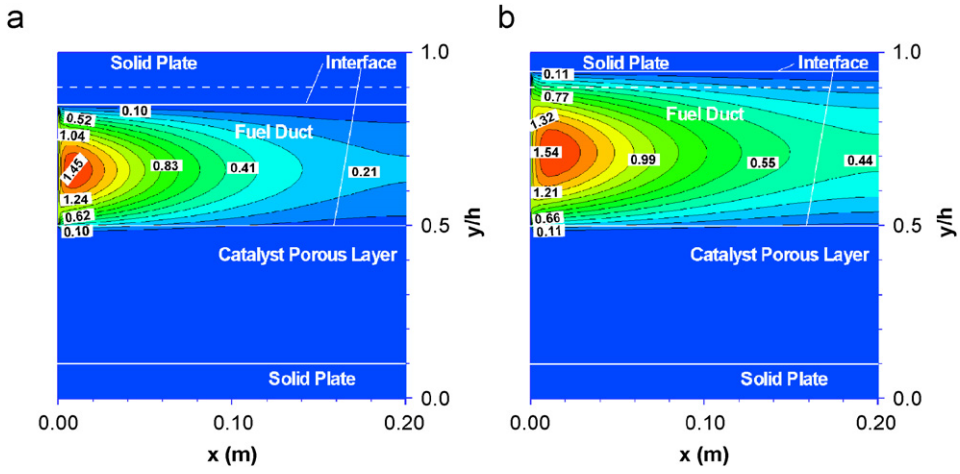

Fig. 2. Velocity contours for the cases of (a) $D_{hr} = 1.17$, (b) $D_{hr} = 0.99$.

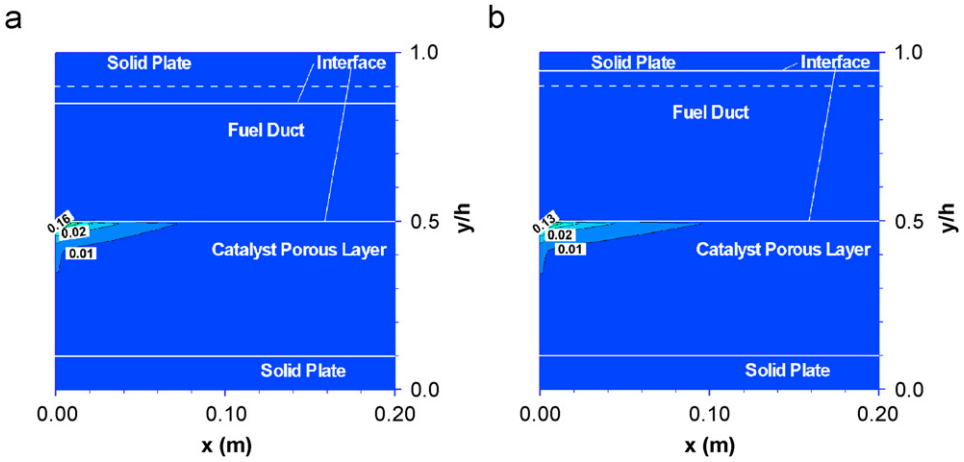

Fig. 3. Distribution of reforming reaction for the cases of (a) $D_{hr} = 1.17$, (b) $D_{hr} = 0.99$.

Table 2
The predicted reactor performance at various diameter ratios

Diameter ratio, D_{hr}	Steam reforming reaction rate $R_{r,max}$, kmol/(m^3 s)	Water gas-shift reaction rate $R_{s,max}$, kmol/(m^3 s)	Reverse methanation reaction rate $R_{re,max}$, kmol/(m^3 s)	Methane conversion, %
1.17	0.173	0.0001	1.230	94.48
1.07 (base case)	0.170	0.0001	1.198	81.69
0.99	0.170	0.0001	1.198	76.16

6.2. *Effects of permeation length ($PL_r = 0.6, 0.9$ vs. 0.8)*

For the base case condition it is expected that the cross-section velocity vectors are dominated by a central and downward flow into the porous catalyst layer from the fuel flow duct. Small downward velocity vectors can be found in most of the porous catalyst layer except at the bottom regions [10]. Because the pressure in the fuel flow duct will fall due to friction, a decreased pressure gradient along the flow direction is expected. Consequently, gas permeation into the porous catalyst layer decreases and becomes weaker. Due to the blockage of the porous layer at the exit, the permeated gas turns up and returns into the fuel flow duct, i.e., the hydrodynamic boundary layer moves back into the fuel flow duct from the porous catalyst layer due to this back permeation [10].

Effects of the permeation length ratio have been investigated by varying the width of the fuel flow duct a, while other ratios were kept constant. Permeation length ratios $PL_r = 0.6$ ($a = 3$ mm) and $PL_r = 0.9$ ($a = 4.5$ mm) were employed, and the predicted performance is compared with each other. From Fig. 4, it is found that the cross-section velocity profiles are similar to each other for different permeation length ratios, in terms of maximum value of the velocity (1.3 m/s) and its distribution. Moreover, the steam reforming reaction rate for the case with small permeation length ratio (maximum reaction rate 0.16 kmol/(m^3 s) in Fig. 5a) is almost in the same order as that achieved in the case with big permeation length ratio (maximum reaction rate 0.15 kmol/(m^3 s) in Fig. 5b). However, the methane conversion efficiency (in Table 3) is high (92.88%) for the latter case, due to its longer permeation length, i.e., longer reaction length. This reveals that the permeation length ratio puts more significant effects on the fuel gas permeation between the fuel flow duct and the porous catalyst layer, and then the methane conversion.

6.3. *Effects of the permeation rate ratio*

The effects of the permeation rate ratio on the fuel gas flow are shown and discussed in this section.

6.3.1. *Permeability ($PR_r = 0.420, 0.010$ vs. 0.042)*

It is noted from Fig. 6a that, by increasing the permeability, fuel gas permeation to the porous layer is big, i.e., the length having a axial velocity in the porous layer close to the fuel flow duct is longer and the maximum value of the velocity in the fuel flow duct is small (1.44 vs. 1.6 m/s), if compared to the case with a small permeability shown in Fig. 6b. This is so because the permeability is a term used for the conductivity of the porous medium with respect to permeation by a fluid. It is known that a big permeability of a porous layer allows more gas to pass at the same pressure gradient. Consequently, more fuel gas is permeated from the fuel flow duct, and the gas convection can be found with bigger velocities in the porous layer close to the fuel flow duct at the entrance region. Certain impacts on the change of the axial velocity distribution are expected for both the fuel flow duct and the porous catalytic layer, when the permeability is large.

From Table 4, it is found that the maximum values of the steam reforming reaction and reverse methanation reaction rates for the case with big permeability ($\beta = 2.0 \times 10^{-9}$ m^2) are

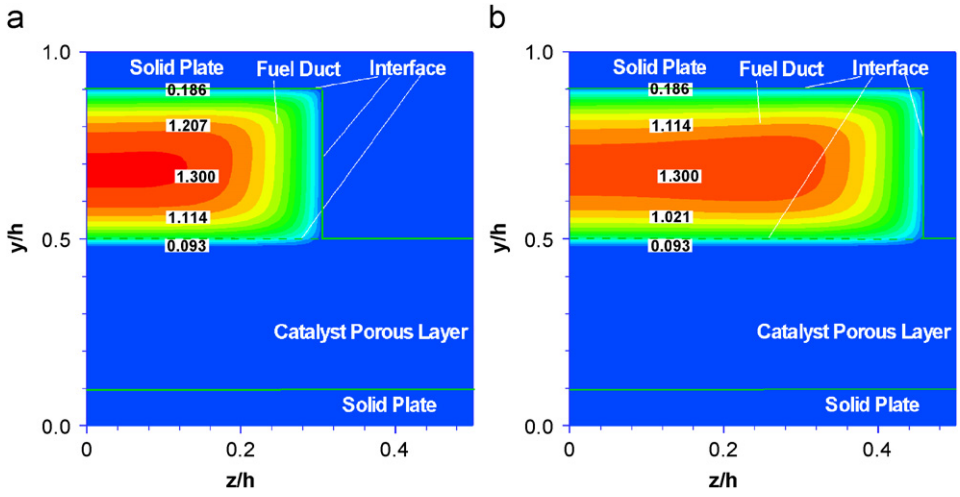

Fig. 4. Distribution of velocity contours at the inlet cross section for the cases of (a) $PL_r = 0.6$, (b) $PL_r = 0.9$.

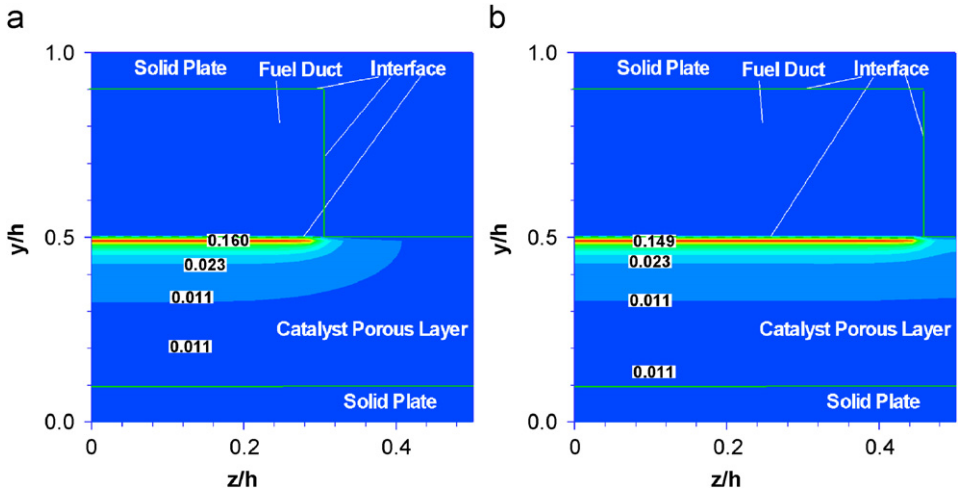

Fig. 5. Distribution of steam reforming reaction at the inlet cross section for the cases of (a) $PL_r = 0.6$, (b) $PL_r = 0.9$.

Table 3
The predicted reactor performance at various permeation length ratios

Permeation length ratio, PL_r	Steam reforming reaction rate $R_{r,max}$, kmol/(m^3 s)	Reverse methanation reaction rate $R_{re,max}$, kmol/(m^3 s)	Methane conversion, %
0.6	0.170	1.200	75.24
0.8 (base case)	0.170	1.198	81.69
0.9	0.170	1.198	92.88

bigger than those achieved in the case with small permeability (5.0×10^{-11} m^2), i.e., 0.282 kmol/(m^3 s) vs. 0.167 kmol/(m^3 s) and 2.432 vs. 1.173 kmol/(m^3 s), respectively. However, the methane conversion efficiencies are almost same in all the cases, i.e., around 80%. This may reveal that big permeability promotes not only CH_4 permeation to the porous catalyst layer for the reactions, but also the unreformed CH_4 back permeation to the flow duct [10]. In overall, permeability effects are significant for both the fuel gas permeation to the porous catalyst layer and the chemical reaction rates.

6.3.2. Effects of inlet velocity ($PR_r = 0.021, 0.084$ vs. 0.042)

Effects of inlet velocity on the reforming performance are shown in Figs. 7 and 8. Permeation rate ratios $PR_r = 0.021$ ($U_{in} = 2.5$ m/s) and $PR_r = 0.084$ ($U_{in} = 10$ m/s) have been employed to compare with the base case, i.e., $PR_r = 0.042$ and $U_{in} = 5$ m/s. It is revealed that, in the entrance region, small PR_r has a small steam reforming reaction rate in Fig. 7a compared to the case in Fig. 7b with a big inlet velocity case, (0.11 vs. 0.21 kmol/(m^3 s) in Fig. 7). It is because the fuel gas flow rate in the fuel flow duct and then to the porous catalyst layer is small in Fig. 7a, as revealed in [10]. Big inlet velocity on the other hand has more significant effects not only on the fuel gases permeation to the porous catalyst layer for the reactions, but also on the convection (the fuel flow rate) in the gas flow duct.

The steam reforming reaction can be found in Fig. 8, represented by a similar hydrogen mole distribution in the duct, particularly in the porous catalyst layer. The porous catalyst layer is occupied by higher H_2 fraction than that in the fuel flow duct resulting from the steam reforming reaction (Eq. (16)), shift

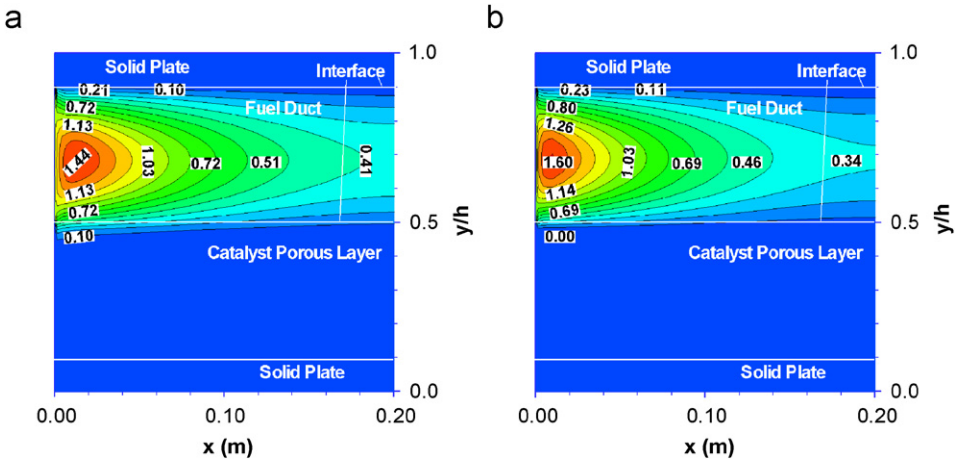

Fig. 6. Effects of the permeation rate ratio (permeability) on the dimensionless axial velocity contours at (a) $PR_r = 0.420$ ($\beta = 2.0 \times 10^{-9}\ m^2$), (b) $PR_r = 0.010$ ($\beta = 5.0 \times 10^{-11}\ m^2$) along the main flow direction of a steam reforming reaction duct.

Table 4
Permeability effects on the predicted reactor performance

Permeability, β	Steam reforming reaction rate $R_{r,max}$, kmol/(m^3 s)	Reverse methanation reaction rate $R_{re,max}$, kmol/(m^3 s)	Methane conversion, %
2.0×10^{-9}	0.282	2.432	79.96
2.0×10^{-10} (base case)	0.170	1.198	81.69
5.0×10^{-11}	0.167	1.173	81.71

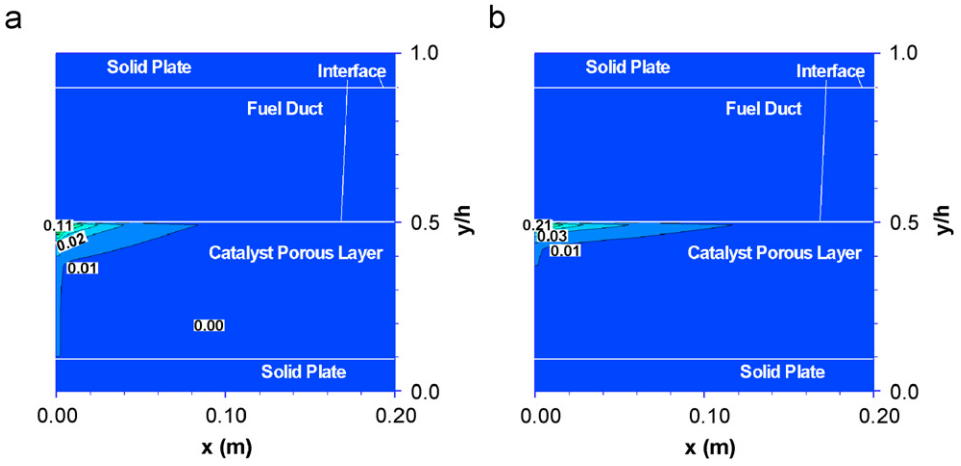

Fig. 7. Effects of the permeation rate ratio (inlet velocity) on the steam reforming reaction distribution at inlet velocity of (a) $PR_r = 0.021$ ($U_{in} = 2.5$ m/s), (b) $PR_r = 0.084$ ($U_{in} = 10$ m/s) along the main flow direction of a steam reforming reaction duct at the base condition.

reaction (Eq. (17)) and reverse methanation reaction (Eq. (18)), as shown in Fig. 8. A large amount of H_2 is produced in the interface region of the porous catalytic layer close to the fuel duct, which is reflected by a sharp increase of the H_2 mole fraction. As revealed in Figs. 3 and 7, the reactions are confined mainly up to around 10% of the overall duct height (i.e., 1 mm) into the porous catalyst layer at most of the stations along the main flow direction, except at the inlet area where the reactions take place more deeply into the porous layer. It is then noted from Fig. 8a that the exit H_2 mole fraction is high even the reforming reaction rate is small compared to the case in Fig. 8b. It means that the H_2 yield and its mole fraction distribution are controlled by the combined effects of the reforming reactions in the porous catalyst layer and the convective flow (the fuel flow rate) along the flow direction downstream the fuel gas flow duct.

6.3.3. Effects of porous layer thickness ($PR_r = 0.084, 0.168$ vs. 0.042)

As expected, thickness of the porous catalyst layer is one of the most important parameters. The effects on the transport

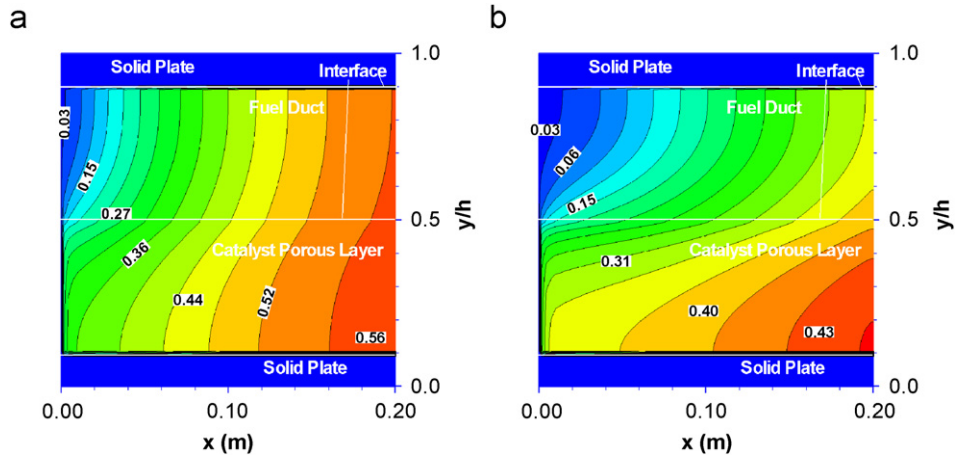

Fig. 8. Effects of the permeation rate ratio (inlet velocity) on the H_2 distribution at inlet velocity of (a) $PR_r = 0.021$ ($U_{in} = 2.5\,m/s$), (b) $PR_r = 0.084$ ($U_{in} = 10\,m/s$) along the main flow direction of a steam reforming reaction duct.

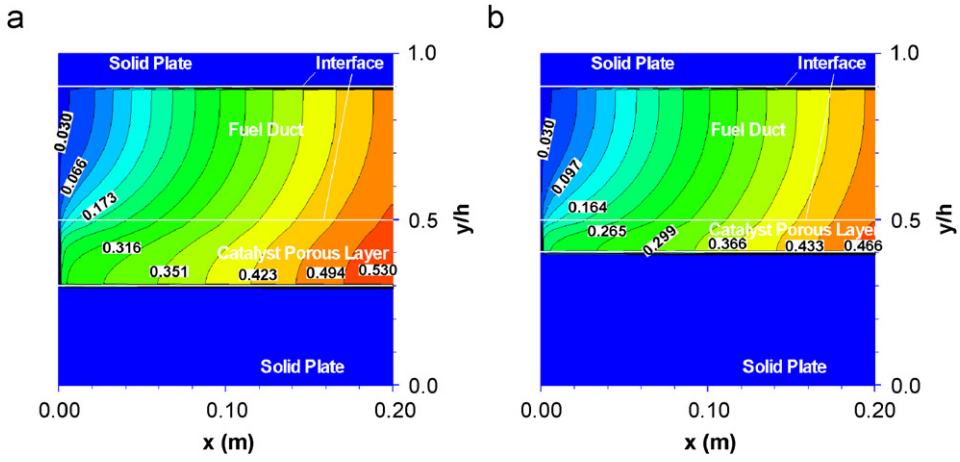

Fig. 9. Effects of the permeation rate ratio (thickness of the porous layer) on the H_2 distribution along the main flow direction of a steam reforming reaction duct at the base condition: (a) $PR_r = 0.084$ ($h_p = 2.0\,mm$), (b) $PR_r = 0.168$ ($h_p = 1.0\,mm$).

Table 5
Effects of the thickness of the porous catalyst layer on the predicted performance

Thickness of the porous catalyst layer, h_p, mm	Steam reforming reaction rate $R_{r,max}$, kmol/(m^3 s)	Reverse methanation reaction rate $R_{re,max}$, kmol/(m^3 s)	Methane conversion, %
4.0 (base case)	0.170	1.198	81.69
2.0	0.121	0.742	82.48
1.0	0.173	1.233	74.12

processes and reforming reaction performance have also been explored in this paper. To do this, the height of porous layer h_p was varied while other parameter ratios were kept constant. It should be mentioned that the thickness of the lower solid plate was changed accordingly to keep the total height of the porous catalyst layer and the lower solid plate constant.

It is noted that the ducts employing thin porous layers (thickness $h_p = 2.0$ and $1.0\,mm$, respectively, vs. $4.0\,mm$) predict very similar H_2 mole fraction profiles in terms of overall distributions, as shown in Fig. 9. However for the case of the thinner porous catalyst layer (Fig. 9b), a smaller H_2 mole fraction ($0.466\,kmol/(m^3\,s)$ in Fig. 9b vs. $0.530\,kmol/(m^3\,s)$ in Fig. 9a) is found in the corner of the porous catalyst layer close to the exit and the bottom solid plate. As revealed in Table 5, a similar methane conversion efficiency is obtained for the case of $PR_r = 0.084$ ($h_p = 2.0\,mm$) if compared to the one obtained at the base condition (i.e., 82.48% vs. 81.69%), but for the case of $PR_r = 0.168$ ($h_p = 1.0\,mm$), the value is low (74.12%).

It is clear that the distribution of steam reforming reaction rates in Fig. 10 holds a similar trend, i.e., strong steam

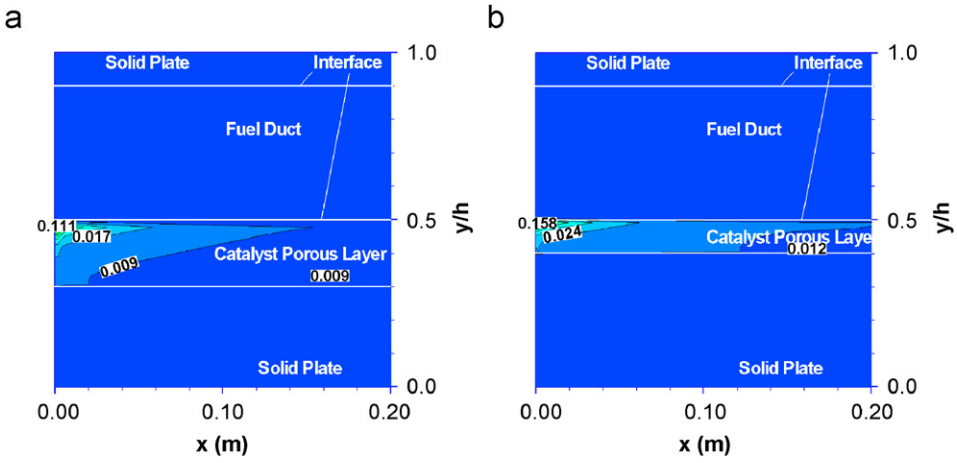

Fig. 10. Effects of the thickness of the porous reforming layer on distribution of steam reforming reaction rate along main flow direction of a reformer duct: (a) $PR_r = 0.084$ ($h_p = 2.0$ mm), (b) $PR_r = 0.168$ ($h_p = 1.0$ mm).

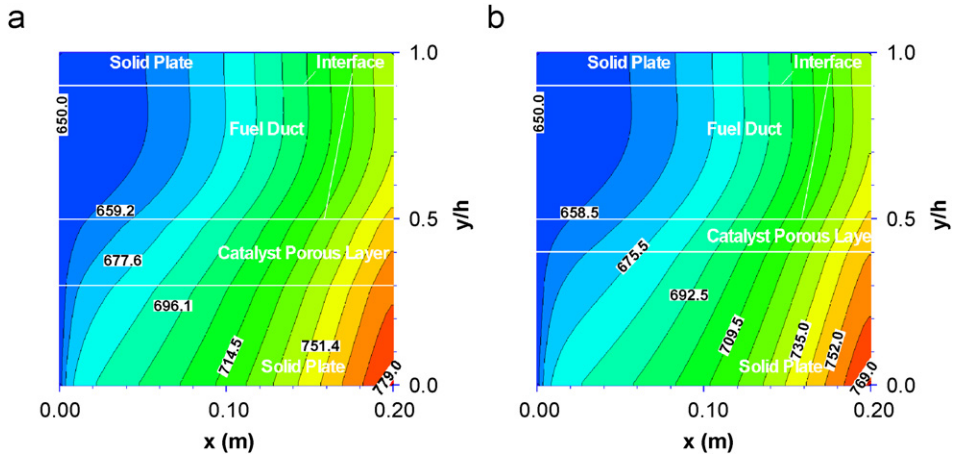

Fig. 11. Effects of the porous catalytic layer thickness on temperature distribution along main flow direction of the duct: (a) $PR_r = 0.084$ ($h_p = 2.0$ mm), (b) $PR_r = 0.168$ ($h_p = 1.0$ mm).

reforming reaction appears in the interface region of the porous catalyst layer close to the fuel flow duct. On the other hand, weak reaction (with small reaction rate value) can be found in the remaining areas as well for the thin porous catalyst layers shown in Fig. 10. The reforming reaction overall performance achieved in the case of $PR_r = 0.084$ ($h_p = 2.0$ mm) is similar to the one for the base case, in terms of H_2 distribution (Fig. 9a) and the methane conversion efficiency (82.48% vs. 81.69% in Table 5), even the maximum values of the steam reforming and reverse methanation reaction rates are smaller ($R_{r,max} = 0.121$ and $R_{re,max} = 0.742$ kmol/(m^3 s) vs. $R_{r,max} = 0.170$ and $R_{re,max} = 1.198$ kmol/(m^3 s), respectively). The maximum values of the steam reforming and reverse methanation reaction rates are somewhat big in the case of $PR_r = 0.168$ ($h_p = 1.0$ mm), however, the methane conversion is small, as shown in Table 5. It is so because the porous catalyst layer is small for the case of $PR_r = 0.168$, in terms of the thickness.

Fig. 11 shows the temperature distribution to reveal the porous layer thickness effects. It is clear that the temperature increases steadily along the main flow direction in Fig. 11. The variation in temperature distribution can also be observed in the vertical direction with a larger value at the bottom solid plate. These are created by the heat flux supplied by the catalytic combustion (modeled by a constant heat flux $q_b = 1000$ J/(m^2 s) in this study). It is found that the reforming ducts employing thin porous layers have high temperatures in both the fuel flow duct and the porous catalyst layers. For instance, the maximum temperatures appearing in the active plate corner (the bottom plate in Fig. 1) at the exit are 779 and 769 °C for thin porous layers, compared to 758.6 °C for the base condition (not shown in this study). It is so because the thin porous catalytic layers are employed to have reforming reactions, where the less heat is consumed by the reforming reactions in Eqs. (16) and (18).

As discussed above, it is clear that the thickness of the porous catalytic layer has opposite roles in the chemical reaction rates and the overall performance in terms of methane conversion. It is due to the fact that the thickness of the porous catalyst

layer is involved in both the diameter ratio and the permeation rate ratio, i.e., a thin porous layer generates a smaller diameter ratio D_{hr}, however, a bigger permeation rate ratio. As a result, the thickness of the porous layer has composite effects on the transport processes and reformer performance. Further study is needed to find an optimal thickness of the porous catalytic layer, in conjunction with the catalyst loading and distribution in the porous layer.

7. Conclusions

In this paper, a fully three-dimensional calculation method has been further developed to study the design and operating parameter effects on transport phenomena coupled by the chemical reactions in a composite duct relevant for a compact reformer. The model offers the possibilities of determining temperature and fuel gas fraction/velocity profiles by taking into account the methane steam reforming, water gas-shift and reverse methanation reactions. The important variables based on reformer duct configurations and operations are grouped into three characteristic ratios. The transport processes and overall reforming reaction performance are then evaluated based on these ratios.

It is found that big diameter ratio and the permeation length ratio have significant effects to yield high methane reforming efficiencies at the exit of the duct. For the permeation rate ratio, another trend is true in terms of the chemical reaction rates, i.e., big permeation rate ratio (high inlet velocity and permeability, and small thickness of the porous catalyst layer) induces big steam reforming and reverse methanation reaction rates. Furthermore, the porous layer thickness has complex effects since it is involved in both the diameter ratio and the permeation rate ratio at the same time, and no simple conclusion can be drawn for the effects on the transport phenomena and overall reforming reaction performance. This study may be used for the reforming duct modeling, as a design tool/adjustment of the duct configuration to establish prescribed flow/reforming conditions and heat transfer, or establish the flow/reforming condition and heat transfer for a given configuration.

Acknowledgment

The Swedish Research Council (VR) and Sida Research Links programme supports the collaboration between Dalian Maritime University and Lund University.

References

[1] Hoang DL, Chan SH. Modeling of a catalytic autothermal methane reformer for fuel cell applications. Appl Catal A 2004;268:207–16.
[2] Samanta I, Shah RK, Wagner A. Fuel processing for fuel cell application, Fuelcell2004-1515. In: Shah RK, Kandlikar SG, editors. Proceedings of fuel cell science, engineering and technology. New York: ASME; 2004.
[3] Farrauto R, Hwang S, Shore L, Ruettinger W, Lampert J, Giroux T. et al. New material needs for hydrocarbon fuel processing: generating hydrogen for the PEM fuel cell. Annu Rev Mater Res 2003;33:1–27.
[4] Dicks AL, Goulding P, Jones SL, Judd R, Ponton K. Assessment of advanced catalyst performance and fabrication options for a compact steam reformer. ETSU F/02/00180/REP, DTI PUB URN 01/1163, UK, 2001.
[5] Zanfir M, Gavriilidis A. Catalytic combustion assisted methane steam reforming in a catalytic plate reactor. Chem Eng Sci 2003;58:3947–60.
[6] Agar DW. Multifunctional reactors: old preconceptions and new dimensions. Chem Eng Sci 1999;54:1299–305.
[7] Yuan J, Ren F, Sundén B. Analysis of chemical-reaction-coupled mass and heat transport phenomena in a methane reformer duct for PEMFCs. Int J Heat Mass Transfer 2007;50:687–701.
[8] Kirillov VA, Kuzin NA, Kulikov AV, Fadeev SI, Shigarov AB, Sobyanin VA. Thermally coupled catalytic reactor for steam reforming of methane and liquid hydrocarbons: experiment and mathematical modeling. Theor Found Chem Eng 2003;37:276–84.
[9] Yuan J, Sundén B. A numerical investigation of heat transfer and gas flow in proton exchange membrane fuel cell ducts by a generalized extended Darcy model. Int J Green Energy 2004;1:47–63.
[10] Yuan J, Rokni M, Sundén B. Three-dimensional computational analysis of gas and heat transport phenomena in ducts relevant for anode-supported solid oxide fuel cells. Int J Heat Mass Transfer 2003;46: 809–21.
[11] Haberman BA, Young JB. Three-dimensional simulation of chemically reacting gas flows in the porous support structure of an integrated-planar solid oxide fuel cell. Int J Heat Mass Transfer 2004;47:3617–29.
[12] Mostinsky IL. Diffusion Coefficient. In: Hewitt GF, Shires GL, Polezhaev YV, editors. International encyclopedia of heat & mass transfer. Florida, USA: CRC Press; 1996.
[13] Ferguson JR, Fiard JM, Herbin R. Three-dimensional numerical simulation for various geometries of solid oxide fuel cells. J Power Sources 1996;58:109–22.
[14] Elnashaie SSEH, Adris AM, Al-ubaid AS, Soliman MA. On the non-monotonic behaviour of methane-steam reforming kinetics. Chem Eng Sci 1990;45:491–501.
[15] Rhie CM, Chow WL. Numerical study of the turbulent flow past an airfoil with trailing edge separation. AIAA J 1983;2:1527–32.
[16] Alazmi B, Vafai K. Analysis of fluid flow and heat transfer interfacial conditions between a porous medium and a fluid layer. Int J Heat Mass Transfer 2001;44:1735–49.